arXiv:1407.4274v2 [cond-mat.mes-hall] 17 Jul 2014

Silicon-carbon bond inversions driven by 60 keV electrons in graphene

Toma Susi,[1,*] Jani Kotakoski,[1,2] Demie Kepaptsoglou,[3] Clemens Mangler,[1] Tracy C. Lovejoy,[4] Ondrej L. Krivanek,[4] Recep Zan,[5] Ursel Bangert,[5] Paola Ayala,[1] Jannik C. Meyer,[1] and Quentin Ramasse[3]

[1] *University of Vienna, Faculty of Physics,*
Boltzmanngasse 5, A-1090 Vienna, Austria
[2] *University of Helsinki, Department of Physics,*
P.O. Box 43, FI-00014 Helsinki, Finland
[3] *SuperSTEM Laboratory, STFC Daresbury Campus,*
Daresbury WA4 4AD, United Kingdom
[4] *Nion Co., 1102 8th Street, Kirkland, Washington 98033, USA*
[5] *School of Materials, The University of Manchester,*
Manchester M13 9PL, United Kingdom[†]

(Dated: October 27, 2021)

Abstract

We demonstrate that 60 keV electron irradiation drives the diffusion of threefold coordinated Si dopants in graphene by one lattice site at a time. First principles simulations reveal that each step is caused by an electron impact on a C atom next to the dopant. Although the atomic motion happens below our experimental time resolution, stochastic analysis of 38 such lattice jumps reveals a probability for their occurrence in a good agreement with the simulations. Conversions from three- to fourfold coordinated dopant structures and the subsequent reverse process are significantly less likely than the direct bond inversion. Our results thus provide a model of non-destructive and atomically precise structural modification and detection for two-dimensional materials.

PACS numbers: 31.15.A-, 61.48.Gh, 68.37.Ma, 81.05.ue

Recent breakthrough developments in imaging and spectroscopy in (scanning) transmission electron microscopy [(S)TEM] have enabled the study of structural modifications that occur very literally at the atomic scale. Due to their low dimensionality, materials such as carbon nanotubes, and especially graphene, have proven ideal for these investigations [1–6]. At the same time, (S)TEM instruments can also be turned into nano-sculpting tools: for example, graphene ribbons with specific geometries [7], or perforations of controlled sizes [8, 9], can be fabricated via adjustments of the local chemistry, electron beam energy and density. Heteroatom doping is another way to tailor the properties of graphene [10], which is otherwise ill suited for many applications due to its lack of an electronic band gap [11]. Exchanging some of the carbon atoms by boron or nitrogen can result in an opening of the gap [12, 13], while localised enhancements of plasmon resonances can be created around single silicon substitutions, which then act as atomic antennae [14]. The ability to directly observe the effect of single dopants is thus of the utmost importance in the further development of nano-engineering.

However, doping changes the effect an electron beam has on the atomic structure of graphene, as we have recently shown for nitrogen substitutions [15]. In that case, the slightly higher mass of nitrogen as compared to carbon leads to an increased likelihood to knock out the carbon atoms next to the dopant than the dopant itself or C in pristine areas. We also predicted that damage would be negligible at a primary beam energy of 60 keV, which was recently confirmed by atomic resolution imaging and electron energy loss spectroscopy (EELS) [5, 6]. Recent studies established that silicon dopants—significantly heavier and larger in covalent radius than either carbon or nitrogen—can bond in two distinct ways within the lattice: a non-planar, threefold coordinated configuration (denoted Si-C_3) where the Si atom replaces a single carbon atom, binding to three neighbouring C and buckles out of the plane; and a planar, fourfold coordinated configuration (Si-C_4) where the Si atom is bonded to four C atoms and occupies a divacancy in the lattice [3, 4]. Although beam damage was occasionally observed, apart from a study on the dynamics of Si_6 clusters in a graphene pore [16], the effects of electron irradiation have not been reported in detail.

In this Letter, we show that structural changes in silicon-doped graphene (Si-graphene) drastically differ from those in nitrogen-doped graphene. For Si-graphene, they predominantly take the form of a random walk by the Si atoms through the lattice, with no other changes in the structure. Through first principles molecular dynamics simulations, we show

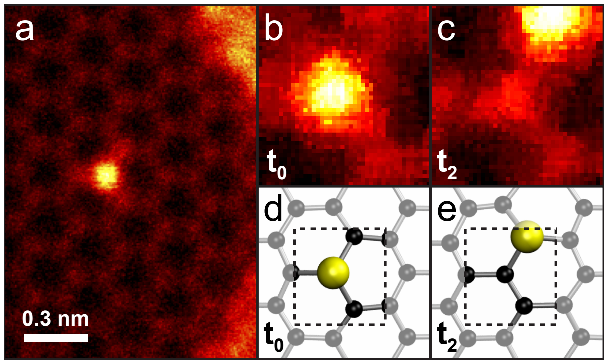

FIG. 1. (Color online) (a) An area of graphene where the bright contrast originates from a single Si-C_3 dopant (high angle annular dark field (HAADF) detector). (b) A closer view of a Si site under continuous 60 keV electron irradiation in a reduced scan window at time t_0 (binned over six exposures of 88 ms, medium angle annular dark field (MAADF) detector). (c) The same area one binned frame (0.5 s) later at time t_2, where the Si atom is observed to have moved by one lattice site (MAADF). (d,e) Structural models where the areas shown in (b,c) are outlined by the dashed lines.

that each step is a result of an electron impact on one of the C atoms neighbouring the Si, and how the non-planarity of the structure plays a crucial role. The probability calculated for this process agrees well with an estimate obtained through a stochastic analysis of the experimental data. We further discuss the few observed events that lead to the conversion of Si-C_3 sites into Si-C_4 ones, and show that they are well accounted for as knock-on damage. The significantly greater probability of the non-destructive reorganisation coupled with its directionality should allow the motion of the Si atoms to be controlled with atomic precision.

Our graphene samples were synthesised by chemical vapour deposition [17], and typically contain a low concentration of silicon incorporated as individual dopants in the lattice [3, 4, 18]. We observed the samples using a Nion UltraSTEM$^{\text{TM}}$100 electron microscope equipped with a cold field emission gun operated at a 60 keV primary beam energy in near-ultrahigh vacuum (2×10^{-7} Pa) [4, 22]. The Si atoms can be directly identified within STEM images by their brighter contrast with respect to the graphene lattice C atoms due to their higher atomic number [19]. The identification has also been verified by atomically resolved EELS [3, 4].

In Fig. 1, we illustrate the predominant beam-induced process, whereby the Si atom is seen to move from one lattice site to the next during continuous imaging with an estimated

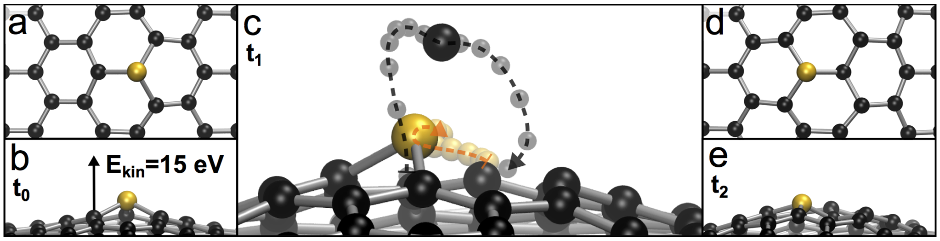

FIG. 2. (Color online) Molecular dynamics simulation of an electron impact delivering 15 eV to a C atom neighbouring Si-C_3 in graphene. (a) Top view of the starting configuration at time t_0. (b) Side view at t_0, with the kinetic energy indicated on the impacted atom. (c) A snapshot at t_1 (∼700 time steps into the simulation), with the entire trajectories of the ejected C atom and the Si atom marked by semi-transparent balls and dotted lines. (d) Top view near the end of the simulation at time t_2 after ∼1400 time steps. (e) Snapshot at time t_2. Note that although the atomic motion has not ceased by this point, no further changes in the atomic configuration follow.

dose rate of 2.2×10^7 $e^-/\text{Å}^2$s. Since atomic motion happens at sub-picosecond timescales, electron microscopy can only capture static snapshots of structures that are in effect fully relaxed. Although processes happening below our experimental time resolution of 88 ms cannot be ruled out, our observations give us a high degree of confidence that we capture the relevant dynamics. The observed events are non-destructive reorganisations of the structure, similar to the process of Stone-Wales transformations that were earlier shown to be due to sub-threshold electron impacts [20], rather than thermally driven bond rotations [21]. The process is also not limited to perfect hexagonal arrangements (see the Supplemental Material [22]).

To gain insight into the dynamics of such processes at the atomic scale, we used density functional theory molecular dynamics (DFT/MD) calculations as described in more detail in Refs. [15, 20, 23]. Although DFT describes the electronic ground state, the atomic dynamics take place over tens to hundreds of femtoseconds, whereas the relevant electron dynamics occur on sub-fs timescales in a metallic system [24]. Ionisation effects were also explicitly ruled out by experiments with ^{12}C and ^{13}C graphene [25]. Thus the ground state approximation is valid to a good degree of accuracy. In high-energy irradiation, the displacement threshold T_d is defined as the minimum kinetic energy required by an atom to be removed from its position in a material. We estimated it by increasing the starting kinetic energy of a target atom until it escaped the structure during the course of an MD simulation. For atomic rearrangements, the same procedure was used to establish threshold limits for a particular reorganisation.

The calculations were performed using the grid-based projector-augmented wave code (GPAW [26, 27]; for details on the computational parameters see Ref. [22]). To speed up the calculations, we used a double-zeta linear combination of atomic orbitals (LCAO) basis. However, we directly compared the calculated knock-on thresholds for C in pristine graphene and the Si atom in Si-graphene with our earlier methodology [28, 29], and established agreement within our computational accuracy. Furthermore, we double-checked the Si jump threshold by full accuracy finite-differences calculations.

The non-planar Si-C_3 configuration can have two distinct positions with respect to the beam direction: the Si atom either protrudes 'below' (in the instrument geometry) the plane towards the incoming beam, or 'above' it along the direction of the beam. These present different T_d and cannot be experimentally distinguished from a 2-dimensional projection of the lattice recorded with a normally incident beam. However, we suspected that the threshold for flipping a Si atom from 'below' to 'above' should not be very high even for 60 keV electrons, as no bonds need to be broken for the transformation. Indeed, a nudged elastic band [30] calculation yields a barrier of only ca. 1.1 eV for this process (see Ref. [22]). Thus all Si configurations are effectively 'above' the graphene plane under observation, and the beam-induced alignment is expected to be thermally stable.

Our simulations yield a T_d of approximately 13.25 eV for the Si atom bonded in the Si-C_3 configuration. However, due to the large mass of Si (28 amu), the probability for 60 keV electrons to transfer this much energy to the dopant is low, resulting in a cross section of 6.6×10^{-7} barn when out-of-plane lattice vibrations with a Debye temperature of 1287 K are taken into account [25]. This agrees well with the observation that Si atoms are rarely lost [3, 4, 16]. The knock-on threshold for one of the three C neighbours to Si is higher, about 16.875 eV, but leads to a much larger cross section ($\sim$ 0.022 barn) due to the lower mass of C (unless otherwise stated, we refer to ^{12}C). This process leads to a conversion Si-C_3 $\rightarrow$ Si-C_4, which can occur at high irradiation doses.

More interesting are impacts below T_d, which nevertheless lead to local changes in the structure. For example, energies between 15.0 and 16.25 eV result in the C atom being ejected from the lattice, but with a trajectory curving first slightly away and then towards the Si due to their mutual interaction. The Si simultaneously relaxes towards the vacated lattice site, as illustrated for the 15 eV-case in Fig. 2 (a movie is available through Ref. [22]). Between 16.5 to 16.75 eV the C atom almost escapes, but is drawn back by the attractive interaction with the Si atom to land on top of the lattice on the side opposite to its starting position, while the remaining structure assumes the Si-C_4 configuration. At 14.5 eV, the ejected C is left as an adatom directly to the side of the Si, but at 14.75 eV, it bounces off the Si atom on its downward trajectory and lands as an adatom on the opposite side. For energies below 14.5 eV, no change in the structure is obtained.

Because Si-C_3 is energetically favoured over Si-C_4 (by ca. 1.02 eV [22]), it is likely that all configurations where the C adatom remains very close will relax back into the Si-C_3 configuration (whether this results in an apparent jump event likely depends on whether C landed on the opposite side). We thus take 14.625 eV to be the lower threshold for this process, corresponding to a cross section of 0.494 barn. To estimate the cross section for moving the Si dopant, we subtract the cross section corresponding to T_d (as the largest cross section is a sum of the cross sections of all possible outcomes), i.e., $0.494 - 0.022 = 0.472$ barn. If we instead assume no recombination of C adatoms with the Si-C_4 site, the cross section estimate is reduced to 0.316 barn. (These would be 0.130 and 0.084 barn for ^{13}C, respectively.) All of the reported results correspond to displacements in a direction perpendicular to the graphene plane, and the curved trajectory is a result of the silicon-carbon interaction.

To double-check the calculated value, we carried out a few computationally demanding simulations using the default GPAW finite differences (FD) mode. The FD calculations gave a slightly lower knock-on threshold of 16.625 eV (0.032 barn), but also a lower flip threshold of 14.375 eV (0.666 barn); the jump cross section would thus be $0.666 - 0.032 = 0.634$ barn [31].

In our experimental data, we found 38 cases where a clear Si jump was observed, with one continuous time series containing 19 consecutive jumps of the same Si atom (Figure 3). The event doses (ie., the irradiation doses between structural rearrangements) determined for the centre of the scan area ranged from 0.24 to 20.01×10^8 $e^-/\text{Å}^2$. However, as the scan frame was centred on the Si atom, the doses on the neighbouring carbon atoms varied from scan to scan, which was taken into account via a Monte Carlo integration. If we assume that the data are stochastic, the waiting times (or, equivalently, the doses) should be Poisson-distributed. Thus the expected value of a Poisson distribution fitted to the data can be used

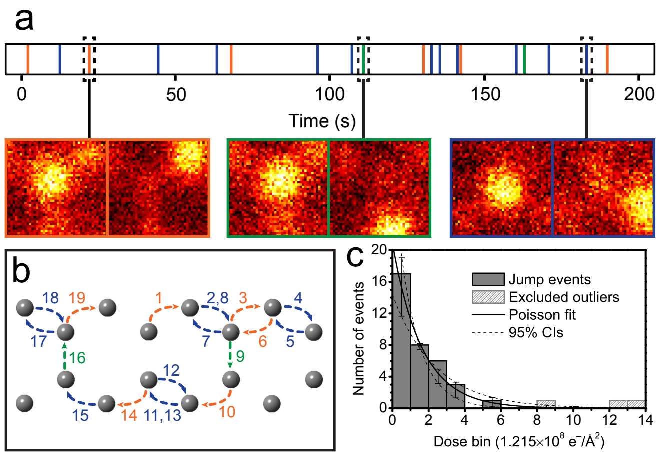

FIG. 3. (Color online) a) An experimental time series of 19 consecutive jumps. Vertical lines mark the observed times of the jumps from the beginning of the experiment. Each event has a colour corresponding to one of the three inequivalent bonds in the lattice over which the jump occurred. b) A schematic illustration of the directions of the jumps in the lattice. Insets: micrographs showing the third, ninth and 18th jump events (MAADF detector, each binned from six consecutive 88 ms frames). c) A histogram of the observed event doses with the optimised binwidth [22]. The solid line is an exponential with the fitted Poisson mean. The excluded outliers are shown in light grey (see text).

to estimate a cross section for the process (see Ref. [22] for details).

We obtained an expectation value of 2.57×10^8 e$^-$/Å^2 for the event dose, with a 95% confidence interval (CI$_{95\%}$) of $[1.59,\ 4.09]\times10^8$ e$^-$/Å^2 [32]. This yields an interaction cross section of 0.389 barn (CI$_{95\%}$ [0.244, 0.629] barn). However, further comparison between the data and the obtained Poisson distribution reveals that three events with the highest doses have a probability lower than 10^{-3} to be a result of the same process. We believe that some of these can be due to ^{13}C atoms incorporated into the graphene lattice (1.1% of all C atoms can be expected to be ^{13}C), or due to a combination of either a jump and an immediate reverse jump or a displacement and refill by an adatom. Reanalysis of the data without the outliers results in a revised expectation value of 1.63×10^8 e$^-$/Å^2 (CI$_{95\%}$ $[1.12,\ 2.37]\times10^8$ e$^-$/Å^2), and a corresponding interaction cross section of 0.613 barn (CI$_{95\%}$ [0.423, 0.893] barn) [33].

The experimental value is in remarkably good agreement with the FD calculation (0.634 barn), and within its CI$_{95\%}$ also with the range of [0.316, 0.472] barn estimated from the more extensive LCAO simulations. Figure 3c shows a histogram of the event doses, which—as expected for a Poisson process—are found to be well described by an exponential with the fitted Poisson mean (apart from an excess of one event in the third bin, and a deficit of one event in the fifth).

Our data also contains eight events where Si-C_3 is transformed into Si-C_4 (see Fig. 4). Taking into account the total experimental dose on trivalent sites (9.71×10^9 $e^-/\text{Å}^2$), we get an estimated cross section of 0.08 barn for this process, in good agreement with the calculated value of 0.066 barn [34]. Interestingly, the knock-on threshold for the four C neighbours of the Si-C_4 was calculated to be 17.125 eV, i.e., slightly higher than that for the threefold site, suggesting that Si-C_4 is more stable towards knock-on damage than Si-C_3. Indeed, a fourfold site was only once observed to damage further by the loss of atoms.

Each of the eight Si-C_4 sites converted back into Si-C_3 with the addition of a carbon atom (see Fig. 4), presumably by adatom diffusion [35, 36] and subsequent recombination into the more stable configuration. Under the non-equilibrium conditions of our experiment, the average lifetime of the Si-C_4 configuration was ca. 70.0 s before recombination. To understand this process, we performed additional structural relaxation simulations of Si-C_4 sites with a single C adatom initially bonded to C-C bridge sites 1–4 bonds away from the Si. We found the total energy of the system with the C adatom at the closest site was $\sim$2.3 eV lower than when the C was three or four bonds away (see Ref. [22] for details). This suggests that there is an attractive force drawing in mobile adatoms into the Si-C_4, possibly contributing to driving the observed recombinations.

Although our analysis relied on the stochastic nature of events when all the area around the Si dopants was irradiated, it should be stressed that due to the ca. 1 Å beam diameter in modern 60 keV aberration-corrected instruments, it is possible to restrict the irradiation to a chosen carbon atom. For example, we estimate that a 1.1 Å beam with a Gaussian profile, centred on a selected C neighbour of the dopant, would deposit $< 0.3\%$ of the irradiation dose on the other two C neighbours. Thus the motion of silicon atoms in the lattice can in principle be controlled with atomic precision. To explore this idea, we calculated the total energies of systems with two Si atoms separated by 1–4 lattice sites, and found that the energies were lower for closer separations. Remarkably, we once also experimentally observed two Si dopants moving under electron irradiation from two sites' separation to become nearest neighbours (see Ref. [22]).

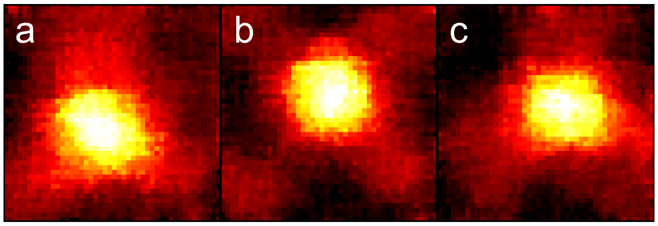

FIG. 4. (Color online) An example of Si-C_3 converting into Si-C_4 and back under 60 keV electron irradiation (HAADF). Frames processed with a Kuwahara noise-reduction filter (5×5 kernel), each an average of six 156 ms frames. The dose rate was estimated to be 2.8×10^7 $e^-/\text{Å}^2$s. (a) The starting configuration showing the Si atom bonded to three neighbours. (b) The same area after three binned frames (2.8 s). A single carbon atom has been removed from the site up from the Si in the image, and the Si has relaxed into fourfold coordination with four carbon neighbours. (c) In the final configuration, the site has reconverted to threefold coordination (after a further three binned frames).

To conclude, we demonstrated how 60 keV electron irradiation causes structural rearrangements at silicon dopant sites in the graphene lattice. Despite appearances, the Si atoms themselves are not perturbed by the electron beam, but undergo a random walk in the lattice due to structural relaxation taking place during a sub-threshold electron impact on a neighbouring carbon atom. The position of this carbon atom thus determines the direction of the walk. Therefore, restricting intense dosing only to a desired carbon atom should allow the motion of the Si atoms to be controlled with atomic precision, and arbitrary arrangements of several Si could plausibly be attained.

We thank CSC Finland Ltd and the Vienna Scientific Cluster for extensive grants of computational resources, and Ask Hjorth Larsen for help setting up the LCAO calculations. T.S. was supported by the Austrian Science Fund (FWF) through grant M 1497-N19, by the Finnish Cultural Foundation, and by the Walter Ahlström Foundation. J.K. was supported by the FWF via M 1481-N20, and by the University of Helsinki Funds. J.C.M. and C.M. acknowledge support from the FWF project P25721-N20 and the European Research Council (ERC) grant PICOMAT. SuperSTEM is the UK National Facility for Aberration-Corrected STEM, supported by the Engineering and Physical Sciences Research Council (EPSRC), who also supported R.Z. and U.B. via grant EP/I008144/1.

---

* toma.susi@univie.ac.at or toma.susi@iki.fi

† Present addresses: R.Z. – Department of Physics, Faculty of Arts and Sciences, Niğde University, 51000 Niğde, Turkey; U.B. – Department of Physics and Energy, University of Limerick, Limerick, Ireland

[1] J. C. Meyer, C. Kisielowski, R. Erni, M. D. Rossell, M. F. Crommie, and A. Zettl, Nano Lett. **8**, 3582 (2008).

[2] K. Suenaga and M. Koshino, Nature **468**, 1088 (2010).

[3] W. Zhou, M. Kapetanakis, M. Prange, S. Pantelides, S. Pennycook, and J.-C. Idrobo, Phys. Rev. Lett. **109**, 206803 (2012).

[4] Q. M. Ramasse, C. R. Seabourne, D.-M. Kepaptsoglou, R. Zan, U. Bangert, and A. J. Scott, Nano Letters **13**, 4989 (2013).

[5] U. Bangert, W. Pierce, D. M. Kepaptsoglou, Q. Ramasse, R. Zan, M. H. Gass, J. A. Van den Berg, C. B. Boothroyd, J. Amani, and H. Hofsäss, Nano Letters **13**, 4902 (2013).

[6] R. J. Nicholls, A. T. Murdock, J. Tsang, J. Britton, T. J. Pennycook, A. Kos, P. D. Nellist, N. Grobert, and J. R. Yates, ACS Nano **7**, 7145 (2013).

[7] Q. Xu, M.-Y. Wu, G. F. Schneider, L. Houben, S. K. Malladi, C. Dekker, E. Yucelen, R. E. Dunin-Borkowski, and H. W. Zandbergen, ACS Nano **7**, 1566 (2013).

[8] Q. M. Ramasse, R. Zan, U. Bangert, D. W. Boukhvalov, Y.-W. Son, and K. S. Novoselov, ACS Nano **6**, 4063 (2012).

[9] S. C. O'Hern, M. S. H. Boutilier, J.-C. Idrobo, Y. Song, J. Kong, T. Laoui, M. Atieh, and R. Karnik, Nano Letters **14**, 1234 (2014).

[10] H. Terrones, R. Lv, M. Terrones, and M. S. Dresselhaus, Rep. Prog. Phys. **75**, 062501 (2012).

[11] A. H. Castro Neto, F. Guinea, N. M. R. Peres, K. S. Novoselov, and A. K. Geim, Rev. Mod. Phys. **81**, 109 (2009).

[12] D. Usachov, O. Vilkov, A. Grüneis, D. Haberer, A. Fedorov, V. K. Adamchuk, A. B. Preobrajenski, P. Dudin, A. Barinov, M. Oehzelt, C. Laubschat, and D. V. Vyalikh, Nano Lett. **11**, 5401 (2011).

[13] Y.-B. Tang, L.-C. Yin, Y. Yang, X.-H. Bo, Y.-L. Cao, H.-E. Wang, W.-J. Zhang, I. Bello, S.-T. Lee, H.-M. Cheng, and C.-S. Lee, ACS Nano **6**, 1970 (2012).

[14] W. Zhou, J. Lee, J. Nanda, S. T. Pantelides, S. J. Pennycook, and J.-C. Idrobo, Nature Nanotechnology **7**, 161 (2012).

[15] T. Susi, J. Kotakoski, R. Arenal, S. Kurasch, H. Jiang, V. Skakalova, O. Stephan, A. V. Krasheninnikov, E. I. Kauppinen, U. Kaiser, and J. C. Meyer, ACS Nano **6**, 8837 (2012).

[16] J. Lee, W. Zhou, S. J. Pennycook, J.-C. Idrobo, and S. T. Pantelides, Nature Communications **4**, 1650 (2013).

[17] X. Li, W. Cai, J. An, S. Kim, J. Nah, D. Yang, R. Piner, A. Velamakanni, I. Jung, E. Tutuc, S. K. Banerjee, L. Colombo, and R. S. Ruoff, Science **324**, 1312 (2009).

[18] T. C. Lovejoy, Q. M. Ramasse, M. Falke, A. Kaeppel, R. Terborg, R. Zan, N. Dellby, and O. L. Krivanek, Applied Physics Letters **100**, 154101 (2012).

[19] O. L. Krivanek, M. F. Chisholm, V. Nicolosi, T. J. Pennycook, G. J. Corbin, N. Dellby, M. F. Murfitt, C. S. Own, Z. S. Szilagyi, M. P. Oxley, S. T. Pantelides, and S. J. Pennycook, Nature **464**, 571 (2010).

[20] J. Kotakoski, J. C. Meyer, S. Kurasch, D. Santos-Cottin, U. Kaiser, and A. V. Krasheninnikov, Phys. Rev. B **83**, 245420 (2011).

[21] L. Li, S. Reich, and J. Robertson, Phys. Rev. B **72**, 184109 (2005).

[22] See Supplemental Material at [url] for details of the simulations; for structural models and details of the total energy calculations; a description of the statistical analyses along with a Wolfram Computable Document Format (http://www.wolfram.com/cdf-player/) Mathematica script; electron micrographs showing two Si atoms moving closer in the lattice, and a Si jump in a graphene grain boundary; and a movie of the simulated Si jump process.

[23] J. Kotakoski, D. Santos-Cottin, and A. V. Krasheninnikov, ACS Nano **6**, 671 (2012).

[24] R. Egerton, Ultramicroscopy **127**, 100 (2013).

[25] J. C. Meyer, F. Eder, S. Kurasch, V. Skakalova, J. Kotakoski, H. J. Park, S. Roth, A. Chuvilin, S. Eyhusen, G. Benner, A. V. Krasheninnikov, and U. Kaiser, Phys. Rev. Lett. **108**, 196102 (2012).

[26] J. Mortensen, L. Hansen, and K. Jacobsen, Phys. Rev. B **71**, 035109 (2005).

[27] J. Enkovaara, C. Rostgaard, J. J. Mortensen, J. Chen, M. Dulak, L. Ferrighi, J. Gavnholt, C. Glinsvad, V. Haikola, H. A. Hansen, H. H. Kristoffersen, M. Kuisma, A. H. Larsen, L. Lehtovaara, M. Ljungberg, O. Lopez-Acevedo, P. G. Moses, J. Ojanen, T. Olsen, V. Petzold, N. A. Romero, J. Stausholm-Møller, M. Strange, G. A. Tritsaris, M. Vanin, M. Walter, B. Hammer,

H. Häkkinen, G. K. H. Madsen, R. M. Nieminen, J. K. Nørskov, M. Puska, T. T. Rantala, J. Schiøtz, K. S. Thygesen, and K. W. Jacobsen, Journal of Physics: Condensed Matter **22**, 253202 (2010).

[28] G. Kresse and J. Furthmüller, Computational Materials Science **6**, 15 (1996).

[29] G. Kresse and J. Furthmüller, Phys. Rev. B **54**, 11169 (1996).

[30] G. Henkelman and H. Jónsson, J. Chem. Phys. **113**, 9978 (2000).

[31] The FD mode should in principle give more accurate forces than the LCAO mode, but the inherent inaccuracy in the numerical integration of the equations of motion in the MD algorithm may render this irrelevant for the actual simulated trajectories. Thus the different values could also be interpreted as an estimate for the inaccuracy of the calculations.

[32] M. Khamkong, Open Journal of Statistics **02**, 204 (2012).

[33] Our average dose per event was 2.55×10^8 e$^-$/Å^2, geometrical mean 1.22×10^8 e$^-$/Å^2. These would have resulted in estimated cross sections of 0.392 and 0.820 barn.

[34] 0.096 barn for the T_D from the FD calculation.

[35] R. Zan, Q. M. Ramasse, U. Bangert, and K. S. Novoselov, Nano Letters **12**, 3936 (2012).

[36] Y. Gan, J. Kotakoski, A. V. Krasheninnikov, K. Nordlund, and F. Banhart, New J. Phys. **10**, 023022 (2008).

Supplemental Material

COMPUTATIONAL UNIT CELL

The unit cell for the molecular dynamics calculations needs to be large enough so that atoms at the edge of the cell do not appreciably move before the ejected atom has either escaped or reached a turning point in its trajectory, as this would cause an overestimation of the restoring forces. In our case a 8×6 graphene supercell of 96 atoms was sufficient.

TOTAL ENERGY CALCULATIONS

All calculations described below were performed in a larger 10×8 unit cell of 160 atoms (+ possible adatoms) to avoid finite size effects, using a $3\times3\times1$ **k**-point grid. The structures were allowed to fully relax without constraints so that the maximum forces were lower than 0.01 eV/Å.

Relative stabilities

The relative stabilities of the Si-C_3 and Si-C_4 configurations were calculated as

$$\begin{aligned} E_{rel} &= E_{form}^{\mathrm{Si-C_3}} - E_{form}^{\mathrm{Si-C_4}} \\ &= (E_{tot}^{\mathrm{Si-C_3}} + E_C - E_{tot}^{\mathrm{gra}} - E_{Si}) - (E_{tot}^{\mathrm{Si-C_4}} + 2E_C - E_{tot}^{\mathrm{gra}} - E_{Si}) \\ &= E_{tot}^{\mathrm{Si-C_3}} - (E_{tot}^{\mathrm{Si-C_4}} + E_C) \end{aligned} \tag{1}$$

where E_{form} denote the formation energies of the two configurations, E_{tot} are their fully relaxed total energies, E_{tot}^{gra} is the total energy of pristine graphene system, E_C is the chemical potential for carbon in graphene (calculated at -9.2232 eV), and E_{Si} is the energy of an isolated Si atom (note that this cancels out in the calculation). This results in a relative energy of -1.023 eV, establishing Si-C_3 as the more stable configuration.

Si-C_3 flipping barrier

The assess the energy barrier for flipping the Si dopant bonded in the Si-C_3 configuration from ‘below’ to ‘above’ the graphene plane, we performed a simple nudged elastic band

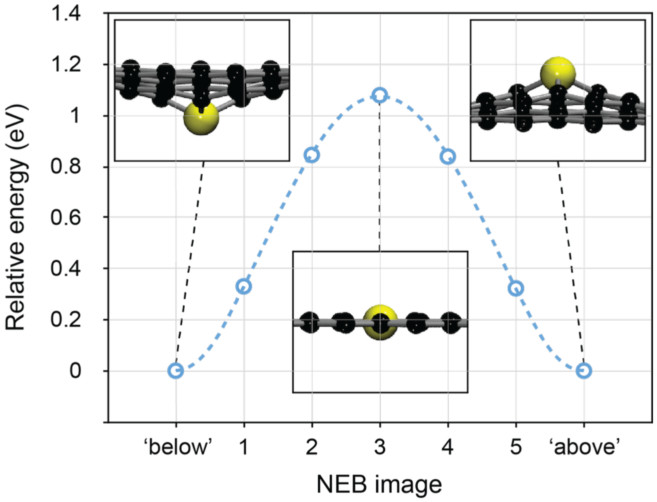

FIG. S1. A nudged elastic band calculation for the energy barrier of flipping the Si-C_3 dopant from 'below' to 'above' the graphene plane. The dotted trendline is a fourth order polynomial fit to the energies, and the insets show the starting, midpoint and final configurations.

calculation (G. Henkelman and H. Jónsson, Journal of Chemical Physics **113**, 9978 (2000)). Since the relaxed starting and ending configurations are symmetric with respect to the graphene plane, the trajectory is a simple line with the maximum energy at the midpoint where the Si atom is in the plane of the lattice. The energy barrier given by the calculation is 1.08 eV (Figure S1), and we also confirmed by a DFT/MD calculation that already a 2 eV starting kinetic energy was sufficient to dynamically induce the flip.

Si-C_4 $\rightarrow$ Si-C_3 reconversion

Since each of the Si-C_4 we observed spontaneously reconverted back into the more energetically stable Si-C_3 configuration—presumably by adatom diffusion and recombination—we studied the energetics of the Si-C_4 defect and a single C adatom (Fig. S2). In the initial configurations, the C adatom was placed on a C-C bridge site 1. . . 4 bonds away from the defect site, and then the structures were fully relaxed. During geometry optimisation, we observed that adatoms placed 1 or 2 bonds away spontaneously moved closer to the defect site, bonding directly with the Si atom. Thus although there seems to be an energy barrier for the recombination that our geometry optimisation could not overcome, there is a clear attractive interaction between the Si-C_4 defect and any diffusing C adatoms in the system.

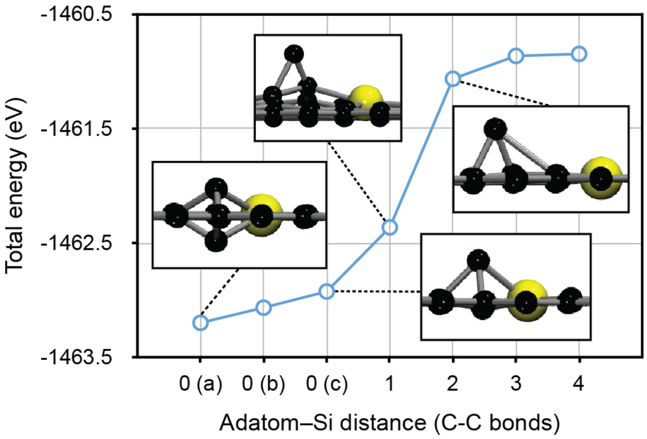

FIG. S2. Total energies of the Si-C_4 system with a single carbon adatom initially placed on a C-C bridge site 1 . . . 4 bonds away from the defect. During relaxation, adatoms placed 1 or 2 bonds away spontaneously relaxed closer to the defect, resulting in several configurations with the C bonded directly to the Si.

Two nearby Si atoms

To explore the possibility of moving several Si dopants close to each other, we calculated the energetics of systems with two Si dopants incorporated into the graphene lattice separated by 1 . . . 4 lattice sites (Figure S3). We found that the energies of the configurations with both Si atoms on either one (unidirectional) or on different (corrugated) sides of the graphene lattice were almost equal, apart from the single lattice site separation, where the corrugated configuration was more stable. Furthermore, the energies were lowered when the two Si atoms were brought closer together, with a shallow energy minimum for the unidirectional configuration found at a two lattice sites' separation.

In one particular instance, we experimentally observed two Si dopants near each other in the lattice (see Figure S4). In the beginning of observation, the Si atoms occupied next nearest neighbour lattice positions. After a certain time of continuous imaging, one of the Si atoms moved one lattice site closer, making the two Si atoms nearest neighbours in the lattice (with one carbon atom possibly removed) This offers direct experimental support for the calculations shown in Figure S3, demonstrating that at least two Si atoms can be brought arbitrarily close.

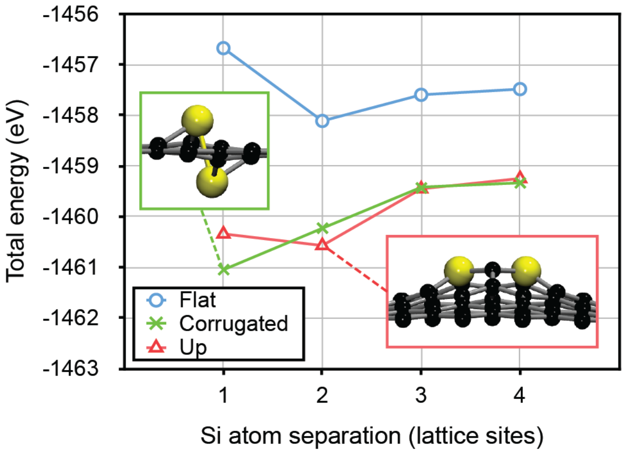

FIG. S3. Total energies of systems with two silicon dopants incorporated into the lattice, separated by 1…4 lattice sites. ‘Flat’ refers to a configuration where both atoms are in the same plane as the graphene lattice (stable but energetically unfavourable), ‘Corrugated’ to where the Si atoms protrude on different sides of the lattice, and ‘Up’ to where both protrude unidirectionally on one side. The insets show the most stable ‘Corrugated’ (green) and ‘Up’ (red) configurations.

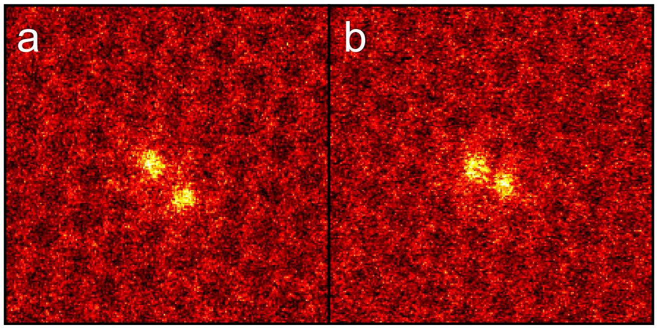

FIG. S4. Two Si dopants initially separated by two lattice sites move closer to each other under 60 keV electron irradiation (HAADF). Each image cropped from an average of six 2.44 second frames covering a larger field of view. (a) The starting configuration shows two bright Si atoms located as next nearest neighbours in the lattice. (b) The same area after a dose of 1.4×10^{7} e^{-}/Å^{2}. The lower right Si atom has moved one lattice site closer, making the two Si dopants nearest neighbours.

STATISTICAL ANALYSES

The doses for the 38 jump events observed in our experimental data can be found in Table I. An illustration of the Monte Carlo integration used to estimate the precise irradiation doses on each of the carbon atoms neighbouring the Si dopant the scan frame was centred on can be seen in Figure S5. If the integration resulted in a proportion of dose larger than 1 on the C atom that jumped (that is, if that C received a higher dose than the Si due to the position of the frame), the precise event dose was simply equal to the experimental dose.

Assuming the jump data are stochastic, the waiting times (or, equivalently, the doses) should arise from a Poisson process with mean λ. Thus the probability to find k events in a given time interval follows the Poisson distribution

$$f(k;\lambda) = \Pr(X = k) = \frac{\lambda^k e^{-\lambda}}{k!}. \tag{2}$$

To estimate the Poisson expectation value, the cumulative doses (calculated by summing the doses incurred by those specific carbon atoms that were observed to jump) given in Table I were combined into a single dataset, which was divided into bins of width w, and the number of bins with 0, 1, 2... occurrences were counted. The binwidth was optimised by

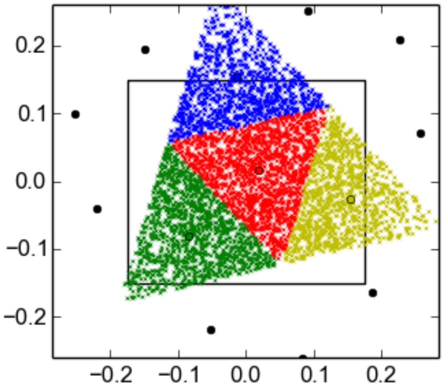

FIG. S5. An example Monte Carlo simulation used to estimate the precise dose on each of the C neighbours to the Si dopant for each frame. The scan frame is denoted by the inner square and the Si atom by the open circle in the centre of the triangle formed from the red dots representing the electrons impinging the Si atom. Electrons impinging on each of the neighbouring three carbon atoms are represented by the blue, green and yellow dots. The axes denote distances in nm.

minimising the Pearson χ^2 statistic calculated between a fitted Poisson distribution and the data (see below). The mean λ was estimated for the dataset by maximising the log-likelihood function of the fit.

An error estimate for the mean was calculated using the approximate confidence interval proposed for Poisson processes with small means and small sample sizes by Khamkong (M. Khamkong, Open Journal of Statistics **02**, 204 (2012)):

$$\mathrm{CI}_{95\%} = \bar{\lambda} + \frac{Z_{2.5}^2}{2n} \pm Z_{2.5}\sqrt{\frac{\bar{\lambda}}{n}}, \tag{3}$$

where $\bar{\lambda}$ is the estimated mean and $Z_{2.5}$ is the normal distribution single tail cumulative probability corresponding to a confidence level of $(100 - \alpha) = 95\%$, equal to 1.96.

The statistical analyses were conducted using the Wolfram Mathematica software, and the Computable Document Format Mathematica script used is included as a Supplemental File. For the entire dataset, a binwidth of 1.06×10^8 e$^-$/Å^2 was found to be optimal, yielding an estimated mean dose of 2.57×10^8 e$^-$/Å^2. However, note that when the experimental cumulative dose data is plotted along with 20 simulated random Poisson processes with the fitted mean, we see that the agreement between the data and the fit is poor due to the influence of high dose events (ie., the outliers) showing as high steps in the cumulative data (see Figure S6).

We then calculated the probabilities that each event was a random event corresponding to a Poisson process with the fitted mean, also shown Table I. This reveals that the three events with the highest doses have probabilities lower than 10^{-3} to be a result of the same process as the rest of the cases. Reanalysis of the data without these outliers results in a revised expectation value of 1.63×10^8 e$^-$/Å^2 (optimal binwidth 1.215×10^8 e$^-$/Å^2). Although the Poisson fit is seemingly slightly less good than with the full dataset, a much better fit between the experimental cumulative doses and the simulated random Poisson processes with the fitted mean can be seen (Figure S7). The expectation value was found to not be very sensitive to the value of the binwidth, provided the chosen width resulted in a good fit.

JUMP IN GRAIN BOUNDARY

Figure S8 shows a Si atom moving by one lattice site along a graphene grain boundary under electron irradiation.

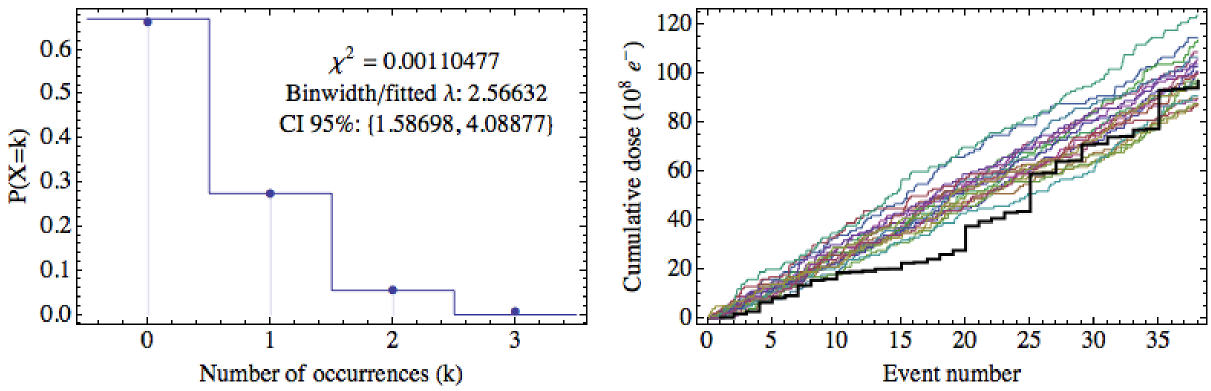

FIG. S6. Poisson analysis of the entire dataset.

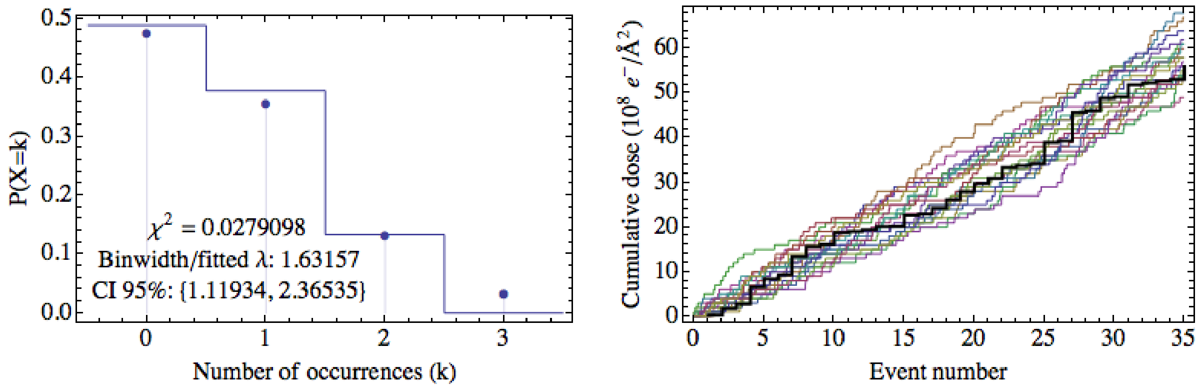

FIG. S7. Poisson analysis of the dataset with the outliers excluded.

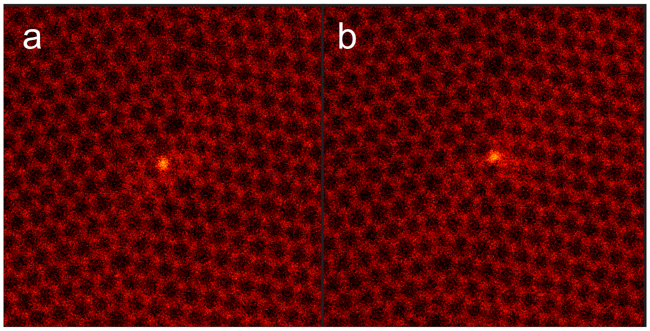

FIG. S8. (Color online) Si atom moving in a graphene grain boundary under 60 keV electron irradiation (MAADF detector). (a) The starting configuration, with the Si atom visible by its brighter Z contrast. (b) The same area imaged after the Si atom had moved by one lattice site along the grain boundary.

TABLE I. Experimental data of the Si jump events. The columns show: binned electron micrograph frame number (0.5 to 0.94 s per frame depending on the experiment); the dose for each event (waiting time multiplied by dose rate); cumulative dose from the start of each experiment; proportion of dose on carbon neighbour number one (C#1; proportion on the Si was by definition 1) estimated by the Monte Carlo calculation; proportion on C#2; proportion on C#3; number of the C atom towards which the Si was observed to jump; precise dose on the C atom that was observed to jump (note that the maximum proportion was set to 1); precise cumulative dose on that C atom; and the probability for this dose assuming a Poisson process with the fitted mean. *Dose per area, in units of $10^8\ \mathrm{e}^-/\text{Å}^2$.

Frame #	**Event dose***	**Cum. dose***	**Prop. on C#1**	**Prop. on C#2**	**Prop. on C#3**	**#C that jumped**	**Precise dose on C***	**Precise cum. dose***	**Poisson probability**
4	0.47	0.47	1.004	0.496	0.404	2	0.23	0.23	0.923
24	2.35	2.81	0.299	0.963	0.641	3	1.50	1.74	0.726
42	2.11	4.93	0.691	0.488	0.733	2	1.03	2.77	0.726
84	4.93	9.85	0.402	0.775	0.675	2	3.79	6.56	0.257
120	2.81	12.66	0.691	0.562	0.652	3	1.83	8.39	0.726
129	1.06	13.72	0.423	0.546	0.886	3	0.94	9.33	0.923
182	6.22	19.94	0.642	0.661	0.595	2	4.10	13.43	0.118
203	2.46	22.40	0.376	0.572	0.895	3	2.19	15.62	0.473
210	0.82	23.22	0.626	0.491	0.778	1	0.52	16.14	0.923
247	4.34	27.56	0.647	0.603	0.653	2	2.60	18.74	0.473
252	0.59	28.14	0.549	0.852	0.473	3	0.28	19.02	0.923
257	0.47	28.61	0.504	0.574	0.836	3	0.39	19.41	0.923
268	1.06	29.67	0.586	0.612	0.679	3	0.72	20.13	0.923
270	0.23	29.90	0.391	0.268	1.364	2	0.06	20.20	0.923
304	3.99	33.89	0.545	0.732	0.607	3	2.43	22.63	0.473
309	0.59	34.48	0.469	0.486	0.917	1	0.28	22.90	0.923
324	2.23	36.70	0.660	0.633	0.601	3	1.34	24.24	0.726
347	2.70	39.40	0.653	0.520	0.725	3	1.94	26.18	0.726
360	2.70	42.10	0.490	0.644	0.754	2	1.73	27.91	0.726

Frame #	**Event dose***	**Cum. dose***	**Prop. on C#1**	**Prop. on C#2**	**Prop. on C#3**	**#C that jumped**	**Precise dose on C****	**Precise cum. dose****	**Poisson probability**
27	10.94	53.04	0.906	0.913	0.957	1	9.91	37.82	3.40×10^{-4}
32	2.03	55.07	0.903	1.028	1.056	1	1.83	39.65	0.726
35	1.22	56.29	1.040	1.099	1.045	3	1.22	40.87	0.726
44	3.65	59.93	0.963	0.741	0.667	3	2.43	43.30	0.473
45	0.41	60.34	0.973	0.994	1.046	3	0.41	43.70	0.923
84	15.40	75.74	2.500	1.429	1.286	1	15.40	59.11	1.53×10^{-8}
86	0.41	76.15	1.086	1.029	1.040	1	0.41	59.51	0.923
97	5.27	81.42	1.003	0.952	0.901	3	4.75	64.26	0.118
191	0.41	81.82	0.800	0.920	0.840	3	0.34	64.60	0.923
207	6.48	88.30	1.013	0.961	0.992	3	6.42	71.02	0.016
208	0.41	88.71	0.966	0.483	0.862	1	0.39	71.41	0.923
215	2.84	91.54	0.993	0.920	1.014	1	2.81	74.22	0.473
216	0.41	91.95	0.750	0.594	0.688	1	0.30	74.52	0.923
295	2.84	94.79	0.960	0.977	1.080	1	2.72	77.25	0.473
296	0.41	95.19	1.083	0.667	1.333	1	0.41	77.65	0.923
335	15.81	111.00	1.034	1.034	1.051	1	15.81	93.46	1.53×10^{-8}
410	0.41	111.41	1.263	0.842	1.316	3	0.41	93.87	0.923
411	0.41	111.81	1.042	1.042	1.208	3	0.41	94.27	0.923
418	2.84	114.65	0.902	1.049	1.049	3	2.84	97.11	0.473